Multi-objective Optimization Design and Performance Evaluation of T-shaped Magnetorheological Brake

Fan Ye, Daoxuan Peng, Yi Yuan, Xin Wang, and Qing Ouyang*

College of Mechanical and Electrical Engineering, Jiaxing University, Jiaxing, 314033 China
*Corresponding author

Abstract: Magnetorheological (MR) intelligent material has been used in vehicle brakes for a long time, which has the advantages of stable control and fast response. However, the MR brakes generally have a large volume to meet the requirement of braking torque. In this paper, the T-shaped MR brake is adopted to increase the output torque, and then the multi-objective optimization analysis is carried out by using Matlab, aiming at the volume, controllability and power consumption of the device. The results show that the volume and power consumption of the device are improved, but the controllability of the device is reduced. The output torque of the brake meets the braking demand, and the power consumption, response time and braking distance are improved.

Keywords: T-shaped; magnetorheological brake; output torque; power consumption; multi-objective optimization

1. Introduction

In recent years, with the rise of smart cars and driverless technology, vehicles are developing towards the integration of electronic control, and the requirements for speed are increasing [1]. Modern cars not only have good maneuverability and comfort, but also have high requirements for safety [2]. When a vehicle runs on a dry, wet, uneven or soft road, it needs different braking forces. However, the traditional brake can't control its output torque to adapt to the road conditions under different conditions, and the traditional brake has a long response time, and the temperature will rise sharply during braking [3,4].

Magnetorheological (MR) smart materials have been widely concerned because of their controllable and adjustable properties, and have been used in new smart vehicle brakes [5,6]. MR fluid can undergo phase change under the action of magnetic field to realize controllable change of fluid viscosity. Therefore, the device can be controlled to output an appropriate and ideal force value by designing a reasonable magnetic circuit. Brakes based on MR materials can be integrated with automobile electronic control system, which can make up for the shortcomings of uncontrollable and slow response time of traditional brakes. Although the MR brake has adjustable output force, how to further optimize its performance from the perspective of structural optimization is the key to design [7,8].

To this end, this paper designs a T-shaped rotary MR brake. According to the requirements of vehicle braking, on the basis of giving priority to ensuring its fast response and torque output, the three objective functions of power consumption, controllability and volume are optimized, and simulation analysis and performance evaluation are carried out by using Matlab.

2. T-shaped MR Brake Structure

T-shaped MR brake structure is shown in Figure 1. Compared with the traditional disc-type MR brake and cylinder-type MR brake, the T-shaped MR brake has the advantages of large working area, simple structure, large output torque, but slightly increased volume. The rotating shaft of the device is made of non-magnetic material, the T-shaped inertia block is made of magnetic pure iron, and the MR fluid is MRF-132DG produced by Lord Company.

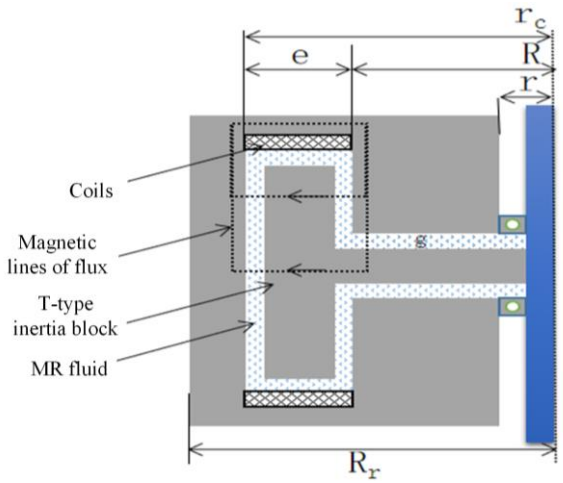

Figure 1. T-shaped MR brake structure.

The working principle of the device is as follows: when the rotating shaft and inertia block start to rotate at the same time, the outer cylinder is still in a static state due to inertia, and there is a speed difference between the rotating shaft and the cylinder. Driven by the viscous friction damping and the Coulomb damping of MR fluid and bushing friction, the outer cylinder will rotate

relatively. When the current is applied to the coil, the device can produce controllable torque and can be adjusted according to the actual situation.

3. Dynamic Model

3.1. Torque Model of T-shaped MR Brake

The constitutive relation of MR fluid characterizes the change of shear stress of MR fluid under different magnetic field intensity and shear strain rate. Bingham model is used to describe the rheological properties of MR fluids, and its constitutive equation [9,10] is as follows:

$$\begin{cases} \tau = \tau_y(\mathrm{H})\,\mathrm{sgn}(\dot{\gamma}) + \eta\dot{\gamma} \mid \tau \mid \geq \tau_y \\ \dot{\gamma} = 0 \mid \tau \mid \geq \tau_y \end{cases} \tag{1}$$

where τ_y is the magnetic shear yield stress of MR fluid; H is the magnetic field strength; $\dot{\gamma}$ is the shear strain rate of MR fluid; η is the post-yield fluid viscosity independent of magnetic field strength.

Before the MR fluid reaches magnetic saturation, the magnetic shear yield stress can be simplified as:

$$\tau_B = \frac{\alpha}{\mu_{mr}} B \tag{2}$$

where μ_{mr} represents the magnetic permeability of MR fluid, and μ_{mr}= 5. B is the magnetic induction intensity. α is a fluid parameter, which is fitted to be α= 0.269 Pa.mm/A.

Ignoring the friction torque caused by sealing, the output torque of the MR brake mainly consists of two parts: viscous torque related to the viscosity of the fluid and controllable Coulomb torque related to the applied magnetic field.

Viscous torque is:

$$\begin{aligned} Tv = \frac{w\pi\eta}{g}\Bigg[& \frac{2(1-\mathrm{c_{sat}})}{c_{sat}}(\mathrm{R}^3 - \mathrm{r}^2\mathrm{R}) + \cdots \\ & \cdots + \frac{2(1-\mathrm{c_{sat}}+\mathrm{c_{sat}}^2)}{c_{sat}}(\mathrm{R} - \frac{r^2}{R})\mathrm{r_c}^2 + (\mathrm{R}^4 - \mathrm{r}^4)\Bigg] \end{aligned} \tag{3}$$

Controllable Coulomb torque is:

$$\begin{aligned} T_{\max} = \frac{\alpha}{\mu_{mr}} B_d \Bigg[& \frac{2\pi}{c_{sat}}\left(R - \frac{r^2}{R}\right)\cdots \\ & \cdots\left(\left(1-c_{sat}\right)R^2 + (1-\mathrm{c_{sat}}+\mathrm{c_{sat}}^2)\mathrm{r_c}^2 + \frac{4}{3}\pi\left(R^3 - r^3\right)\right)\Bigg] \end{aligned} \tag{4}$$

where, B_{d} is the expected magnetic field strength of MR fluid, where B_{d} is 0.5 T. c_{sat} is the ratio of the expected saturation magnetic induction intensity of MR fluid to the saturation magnetic induction intensity of ferromagnetic material. w is the rotor angular velocity. R is the coil inner diameter. r_{c} is the coil outer diameter. e is the radial thickness of the cylinder.

3.2. Vehicle Braking Dynamic Model

The maximum braking torque M_1 of the front wheel and the maximum braking torque M_2 of the rear wheel are as follows:

$$\begin{cases} M_1 = \left(\dfrac{mgb}{L} + \mathrm{m}\dfrac{dv}{dt}\dfrac{h_g}{L}\right)\mu\,\mathrm{R_r} \\ M_2 = \left(\dfrac{mga}{L} - \mathrm{m}\dfrac{dv}{dt}\dfrac{h_g}{L}\right)\mu\,\mathrm{R_r} \end{cases} \tag{5}$$

In which dv/dt is 6.2m/s^2, and other parameters are shown in the following Table 1:

Table 1. Initial design parameters of MR device.

Item	Symbol	Unit	value
total mass	m	kg	1014
Wheelbase	L	mm	2515
Centroid height	hg	mm	685
Horizontal distance from centroid to front axle	a	mm	1260
Horizontal distance from centroid to rear axis	b	mm	1255
Front axle load	mf	kg	506
Rear axle load	mr	kg	508
Rolling radius of wheel	Rr	mm	273
Tyre type	165/70R13		

4. Optimal Design of MR Device

4.1. Optimization Objective

In order to ensure the dynamic performance, controllability and fast response of vehicle brakes, the optimization objectives are as follows:

Sub-optimization objective 1: The power consumption of MR brake should be as small as possible.

Sub-optimization objective 2: Minimum friction torque.

Sub-optimization objective 3: Minimum volume.

Sub-optimization objective 4: Optimal controllability of brake.

Sub-optimization objective 5: Maximum output controllable torque.

The above 5 optimization objectives are expressed as follows:

$$\min\begin{cases} P\max = \dfrac{8\pi r_b kvgB_d}{u} \\ Tv = \dfrac{w\pi\eta}{g}\left[\dfrac{2(1-\mathrm{c_{sat}})}{c_{sat}}(\mathrm{R}^3 - \mathrm{r}^2\mathrm{R}) + \dfrac{2(1-\mathrm{c_{sat}}+\mathrm{c_{sat}}^2)}{c_{sat}}(\mathrm{R} - \dfrac{r^2}{R})\mathrm{r_c}^2 + (\mathrm{R}^4 - \mathrm{r}^4)\right] \\ V\max = 2\pi(\mathrm{r_c}^2 + \mathrm{R}^2 - r^2)\left(\dfrac{R^2 - r^2}{2R}\dfrac{1+c_{sat}^2}{c_{sat}} + \dfrac{2gB_d}{\mu_{mr}ve} + \mathrm{g}\right) \\ -\mathrm{K} = -\dfrac{T\max}{Tv} \\ -T\max = -\dfrac{\alpha}{\mu_{mr}}B_d\left[\dfrac{2\pi}{c_{sat}}\left(R - \dfrac{r^2}{R}\right)\left(\left(1-c_{sat}\right)R^2 + (1-\mathrm{c_{sat}}+\mathrm{c_{sat}}^2)\mathrm{r_c}^2 + \dfrac{4}{3}\pi\left(R^3 - r^3\right)\right)\right] \end{cases} \tag{6}$$

4.2. Constraint Condition

Optimization constraints include the magnetic induction intensity constraints and the performance constraints, as shown in the following equations:

The magnetic induction intensity constraints:

$$\begin{cases} \left(R^2 + 2RL_3\right)B_d - B_{fer}(\mathrm{R}^2 - \mathrm{r}^2) \leq 0 \\ \left(R^2 + 2RL_3\right)B_d - B_{fer}((\mathrm{r_c} + 0.01)^2 - \mathrm{r_c}^2) \leq 0 \end{cases} \tag{7}$$

Considering the output torque and response time of the device, the constraints to be met are as follows:

$$\begin{cases} (\frac{Gb}{L}+\frac{\text{mah}_g}{L})\mu \text{Rr}-\text{Tmax}-\text{Tv}\le 0 \\ \frac{R^2-r^2}{c_{sat}kv\left(r_c+\text{R}\right)}B_d-0.015\le 0 \end{cases} \quad (8)$$

where k is the coil resistivity and v is the current density.

4.3. Design Variable

The design variables of the MR device and their value ranges are shown in the Table 2:

Table 2. Design variables of the MR device.

Design variable	Lower limit /m	Upper limit /m
Coil inner diameter/R	0.05	0.1
Outer diameter of bearing/r	0.01	0.06
Radial thickness of drum/e	0.08	0.2
Damping gap/g	0.0005	0.002

5. Optimization Result Analysis

In this paper, the *fgoalattain* function of Matlab software is used for multi-objective optimization, and its calling format is as follows:

[*x*,*fval*]=*fgoalattain* (*fun, x0, goal, weight, A, b, Aeq, lb, ub,nonlcon*)

In which *fun* is the objective function, *x0* is the initial value of optimization, *goal* is the target value, *weight* is the optimization weight, *A* and *b* are linear inequality constraint matrices, *Aeq* and *beq* are linear equality constraint matrices, *lb* is the lower limit of variable, *ub* is the upper limit of variable and *nonlcon* is the nonlinear constraint.

The comparison of design parameters before and after optimization are shown in the following Table 3:

Table 3. Comparison of design parameters before and after optimization.

Design parameter	Before optimization /m	After optimization /m
Coil inner diameter/*R*	0.07	0.054
Outer diameter of bearing/*r*	0.04	0.010
Radial thickness of drum/*e*	0.1	0.135
Damping gap/*g*	0.001	0.00054

When the frequency is 1Hz and the current is 1.5A, the performance comparison of MR brake before and after optimization is as follows:

Table 4. Comparison of performance parameters before and after optimization.

Performance parameters	Before optimization /m	After optimization /m
Power consumption/$P_{\max}$	184.25 W	119.4 W
Controllability/*k*	3.83	2.05
Volume/$V_{\max}$	0.0199 m^3	0.016 m^3
Response time/q_t	25.1 ms	15 ms
Total torque/*T*	780.8 N.m	720.8 N.m

It can be seen from Table 4 that the MR brake before optimization has better controllability, but it has higher power consumption, slower response and larger volume. After optimization, the power consumption of the device is reduced from 184.25 W to 119.4 W, the response time is increased by 40.23% to 15ms, and the volume of the device is reduced by 20.52% to 0.016 m^3. The controllability of the device is 2.05, which meets the requirements of general engineering applications while taking into account the performance indexes such as volume, power consumption and response time.

Under different ground conditions and input currents, the relationship between ground adhesion coefficient and response time and power consumption of devices before and after optimization is simulated and analyzed, as shown in the Figure 2~3. It can be seen from the Figure 2~3 that the response time of the optimized device decreases, and its response time changes smaller than that of the original device with the change of pavement adhesion coefficient, and its safety performance is higher; After optimization, the power consumption is smaller, and with the change of road adhesion coefficient, the power consumption changes smaller than the original device, and the heat production is less, and the economy and safety are higher.

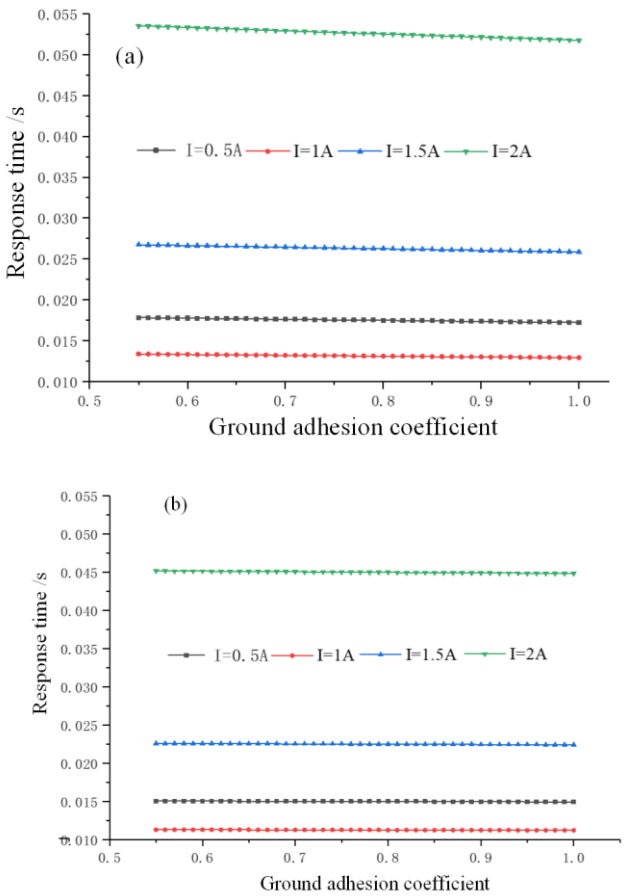

Figure 2. Relationship between ground adhesion coefficient and response time. (a) Before optimization; (b) After optimization.

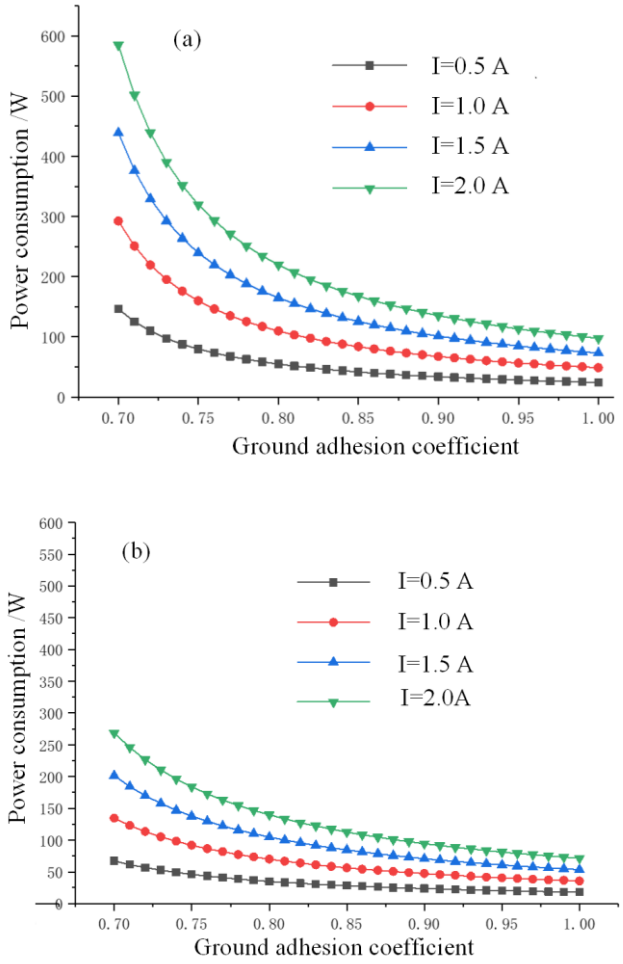

Figure 3. Relationship between ground adhesion coefficient and power consumption. (a) Before optimization; (b) After optimization.

6. Conclusions

The multi-objective optimization design of T-type MR brake device is carried out by using Matlab software, taking into account the performance indexes such as device volume, controllability and power consumption, so that the device can meet the best comprehensive performance. Specific conclusions are as follows:

(1) The T-shaped MR clutch without optimization design has an output torque of 780.8 Nm and a controllability coefficient of 3.83, which means that the designed device can better meet general engineering applications. But at the same time, the device before optimization is still insufficient in energy consumption economy, responsiveness and simplicity, which leads to poor comprehensive performance.

(2) Considering the performance indexes of the device such as output torque, controllability, volume, power consumption and response time, the structure of the device is optimized by Matlab optimization module. The optimized device reduces the power consumption by 35.2%, reduces the volume by 20.52% and improves the response speed to 15 ms, making the comprehensive performance of the device better than that before optimization.

Acknowledgment

This work was supported in part by the Key SRT project funded by the Jiaxing University under Grant CD8517193008, and in part by the Natural Science Foundation of China (NSFC) Grant funded by Chinese Government under Grant 51805209.

References

[1] Rao, Y.T.; Yang, F. Research on path tracking algorithm of autopilot vehicle based on image processing. *International Journal of Pattern Recognition and Artificial Intelligence* **2020**, 34, 117-132.

[2] Xie, G.Q.; Li, Y.W.; Han, Y.B.; Xie, Y.; Zeng, G. Li, R.F. Recent advances and future trends for automotive functional safety design methodologies. *IEEE Transactions on Industrial Informatics* **2020**, 16, 5629-5642.

[3] Patel, S.R.; Upadhyay, R.V.; Patel, D.M. Life-cycle evaluation of anisotropic particle-based magnetorheological fluid in MR brake performance. *Brazilian Journal of Physics* **2020**, 50, 525–533.

[4] Binyet, E.M.; Chang, J.Y. Magnetohydrodynamics modelling of a permanent magnets activated MRF clutch–brake. *Microsystem Technologies* **2020**, 2, 1-10.

[5] Wu, J.; Hu, H.; Li, Q.T.; Wang, S.; Liang, J. Simulation and experimental investigation of a multi-pole multi-layer magnetorheological brake with superimposed magnetic fields. *Mechatronics* **2019**, 65, 102314.

[6] Acharya, S.; Kumar, H. Investigation of magnetorheological brake with rotor of combined magnetic and non-magnetic materials. *SN Applied Sciences* **2019**, 1, 991-997.

[7] Olivier, M.; Sohn, J.W. Design and geometric parameter optimization of hybrid magnetorheological fluid damper. *Journal of Mechanical Science and Technology* **2020**, 34, 2953-2960.

[8] Khanouki, M.A.; Sedaghati, R.; Hemmatian, M. Multidisciplinary design optimization of a novel sandwich beam-based adaptive tuned vibration absorber featuring magnetorheological elastomer. *Materials* **2020**, 13, 2261.

[9] Singh, A.; Thakur, M.K.; Sarkar, C. Design and development of a wedge shaped magnetorheological clutch. *Proceedings of the Institution of Mechanical Engineers Part L Journal of Materials Design and Applications* **2020**, 234, 1252-1266.

[10] Sun, W.; Haiyan, H.U.; Weng, J. Design, testing and modeling of a magnetorheological damper with stepped restoring torque. *Journal of intelligent material systems and structures* **2006**, 17, 335-340.